Supporting Information for

Tree-root mimicked Janus evaporator for solar evaporation of saturated saline water

Zhaolong Wang[a], Ziheng Zhan[a], Yinfeng Li[a], Mingzhu Xie[a], Hui Kong[b], Huigao Duan[*a], Yongping Chen[c, *d]

[a] Interdisciplinary Research Center of Low-carbon Technology and Equipment, College of Mechanical and Vehicle Engineering, Hunan University, Changsha 410082, PR China
[b] School of Mechanical Engineering, Beijing Institute of Technology, Beijing 100081, China
[c] Key Laboratory of Energy Thermal Conversion and Control of Ministry of Education, School of Energy and Environment, Southeast University, Nanjing 210096, PR China
[d] Jiangsu Key Laboratory of Micro and Nano Heat Fluid Flow Technology and Energy Application, School of Environmental Science and Engineering, Suzhou University of Science and Technology, Suzhou, Jiangsu 215009, PR China
* Corresponding authors, Emails: duanhg@hnu.edu.cn (H.D.); ypchen@seu.edu.cn (Y.C.)

This file includes:

Other Supplementary Materials for this manuscript include the following:

Section S1. Salt rejecting performance of poplar trees in nature

Poplar trees always live in the saline-alkali soil, contributing to preventing of wind and sands, regulating climate of oases as well as biodiversity maintenance. As presented in Fig. S1, photosynthesis occurs in the leaves, and the salt will be transported to the trunk through special urinary salt system, which demonstrates an excellent salt rejecting capability.

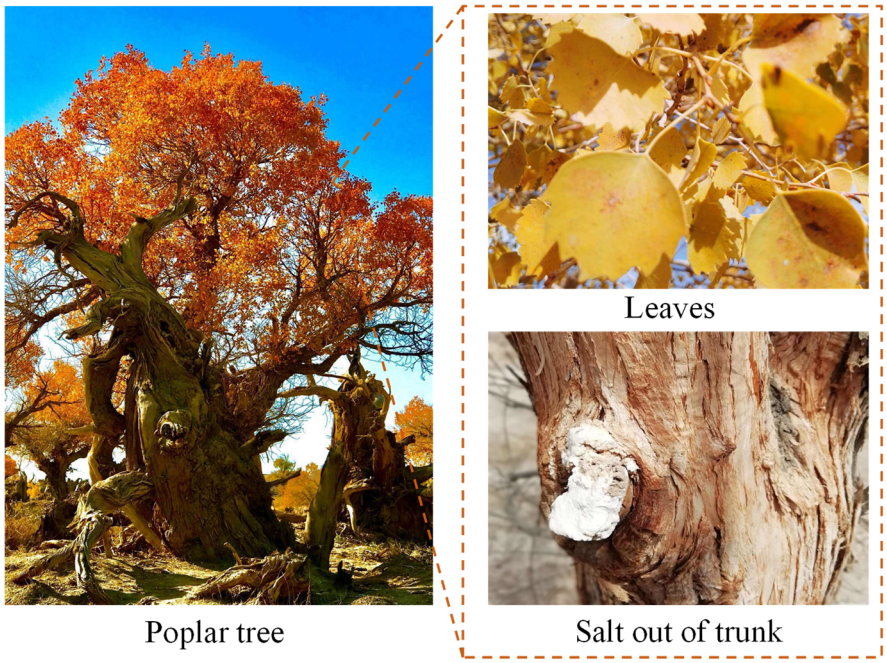

Fig. S1 Salt rejecting performance of poplar trees in nature

Section S2. 3D printing process of bionic evaporators

The 3D printing process of bionic evaporators is shown in Fig. S2. The 3D model of bionic structures is firstly designed with a CAD software and then sliced to several 2D images. Afterwards, those 2D images are sent to a 3D printer to achieve a layer-by-layer printing. After cleaning by deionized water and alcohol for three times, the sample is blown by nitrogen to clean residual resin and dust.

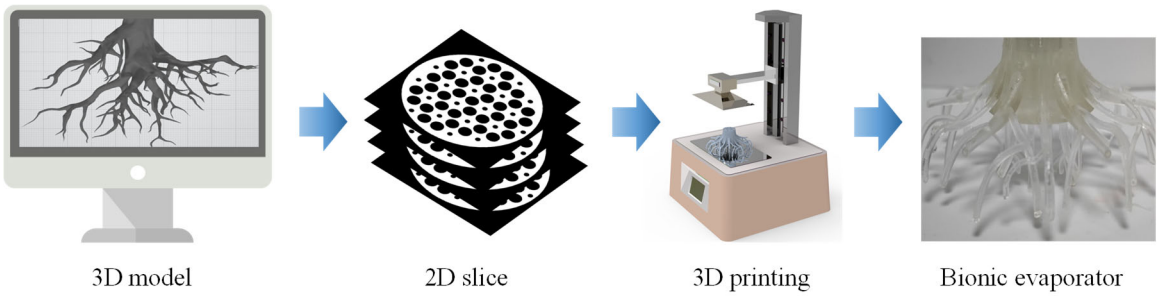

Fig S2 3D printing process of bionic evaporators

Section S3. Characterization of carbon nanoparticles

The SEM image of carbon nanoparticles is shown in Fig. S3, it can be obtained that the diameter of carbon nanoparticles is about 10 nm.

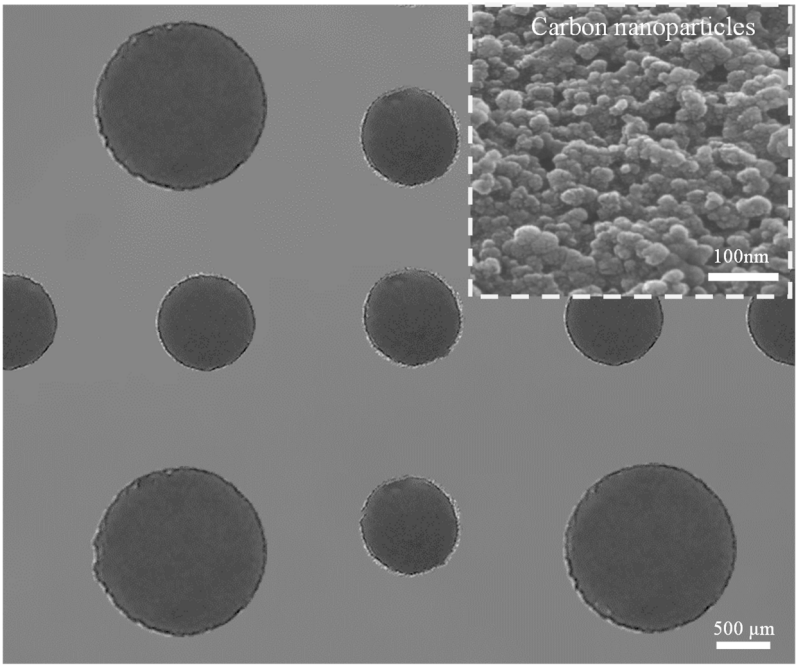

Fig. S3 SEM image of carbon nanoparticles

Section S4. Water transportation process inside microchannels

As presented in Fig. S4, due to the capillary force inside the microchannel, bulk water can be transported from bottom to the top of the evaporators. The speed of transportation for water is about 35 mm/s.

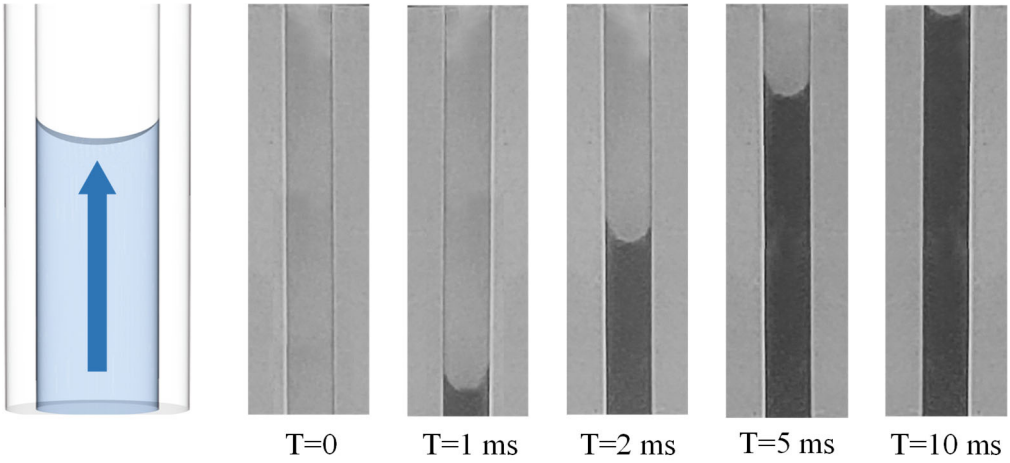

Fig. S4 Water transportation process inside microchannels

Section S5. The set-up for solar water evaporation

The whole evaporation system consists of sunlight simulator, solar vapor generator and clean water collector. The electrical balance can record the mass loss during the whole solar vapor generation and collection process.

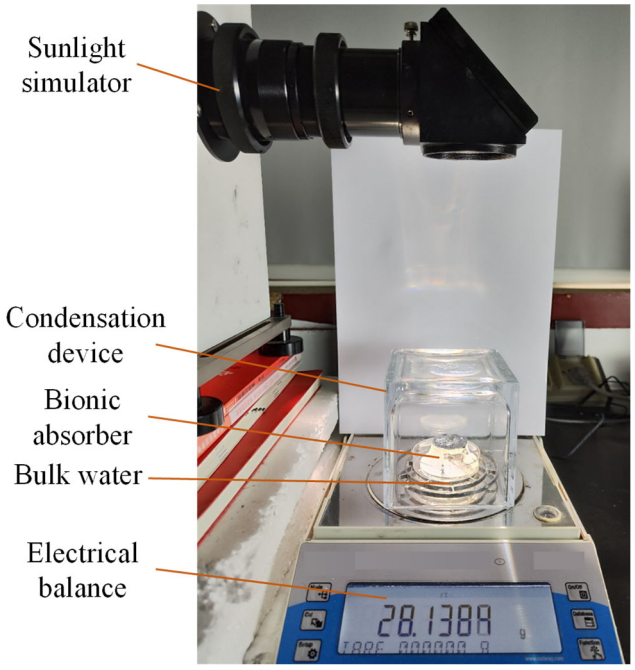

Fig. S5 The whole set-up for solar water evaporation

Section S6. The temperature changes of absorber surface with different arrangements of microchannels and macrochannels.

With the number of macrochannels increasing, water can be transported back to bulk water easier, leading to a better heat sinking capability, thus the temperature of surface will be lowered.

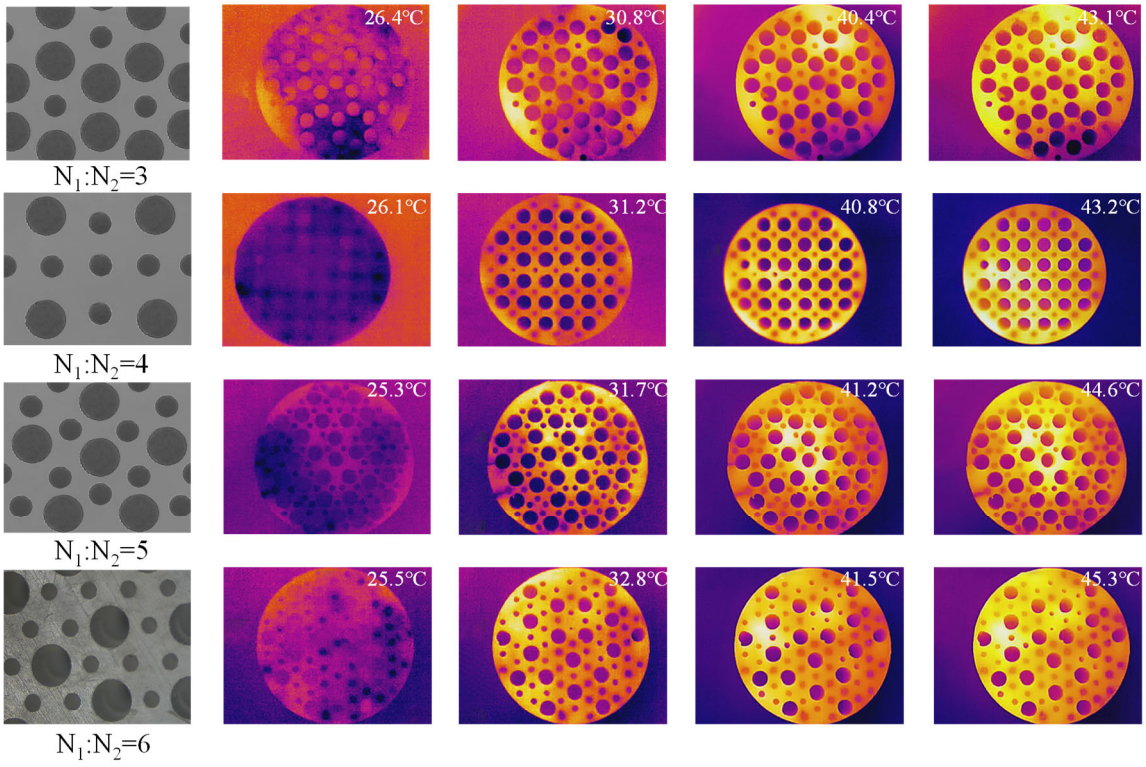

Fig. S6 The temperature changes of absorber surface with different arrangements of microchannels and macrochannels.

Section S7. The temperature changes of absorber surface with different salinity of water

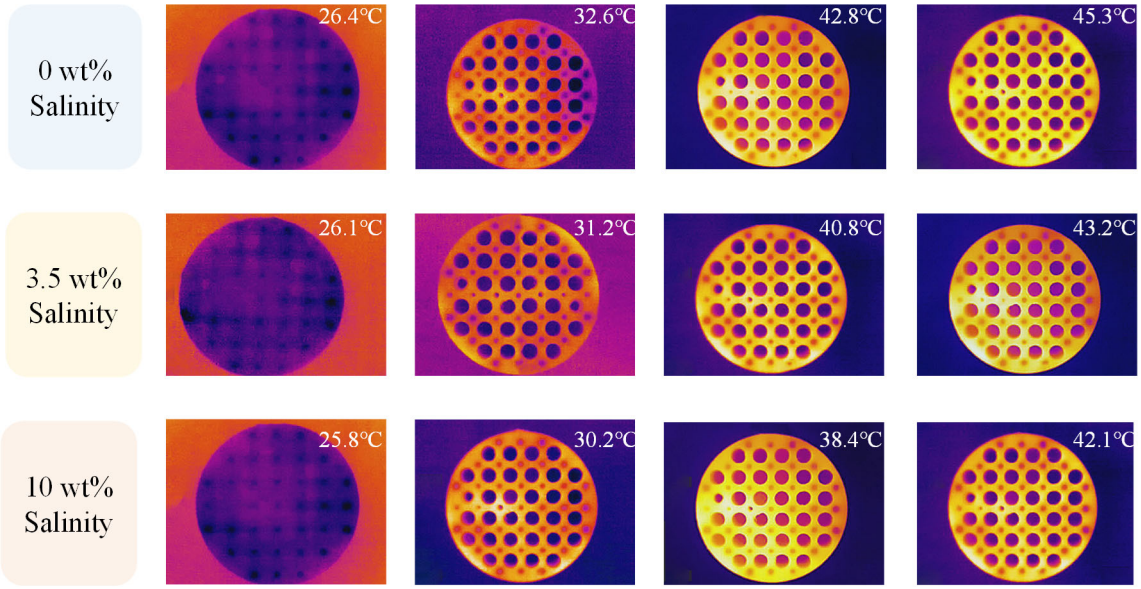

Fig. S7 The temperature changes of absorber surface with different salinity of water.

The surface temperature of our solar evaporators will decrease a little with the increasing salinity of water.

Section S8. Purification of bulk water with metal ions

The purification of bulk water with different metal ions is tested. It can be obtained that the color of the solution will disappear, demonstrating the excellent purification capability of the evaporation system.

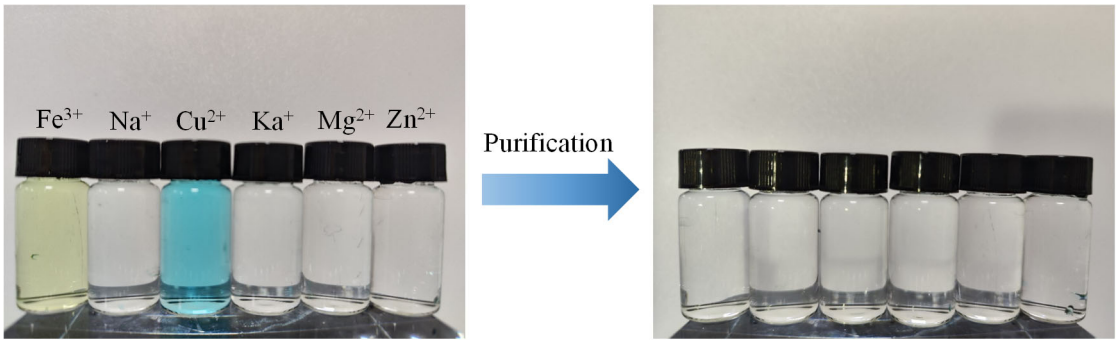

Fig. S8 Purification of bulk water with metal ions

Section S9. Purification of bulk water with organic dyes

The purification of bulk water with different organic dyes is also tested. It can be obtained that color of the solutions will disappear, demonstrating the excellent purification capability of the evaporation system.

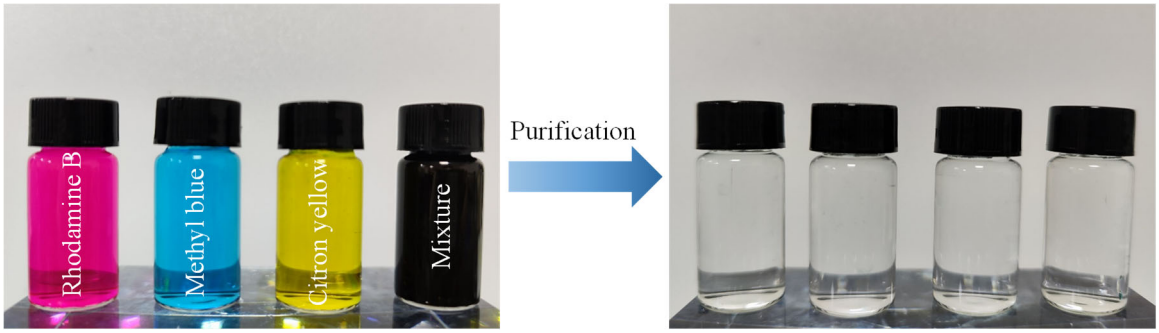

Fig. S9 Purification of bulk water with different organic dyes.

Section S10. Design of different assignments of microchannels and macrochannels

The different assignments of microchannels and macrochannels are shown in Fig. S10. The macrochannel is surrounded by several microchannels with the assignments of N_1:N_2 vary from 2 to 8. The radio of microchannel and macrochannel are 400 μm and 1000 μm, respectively.

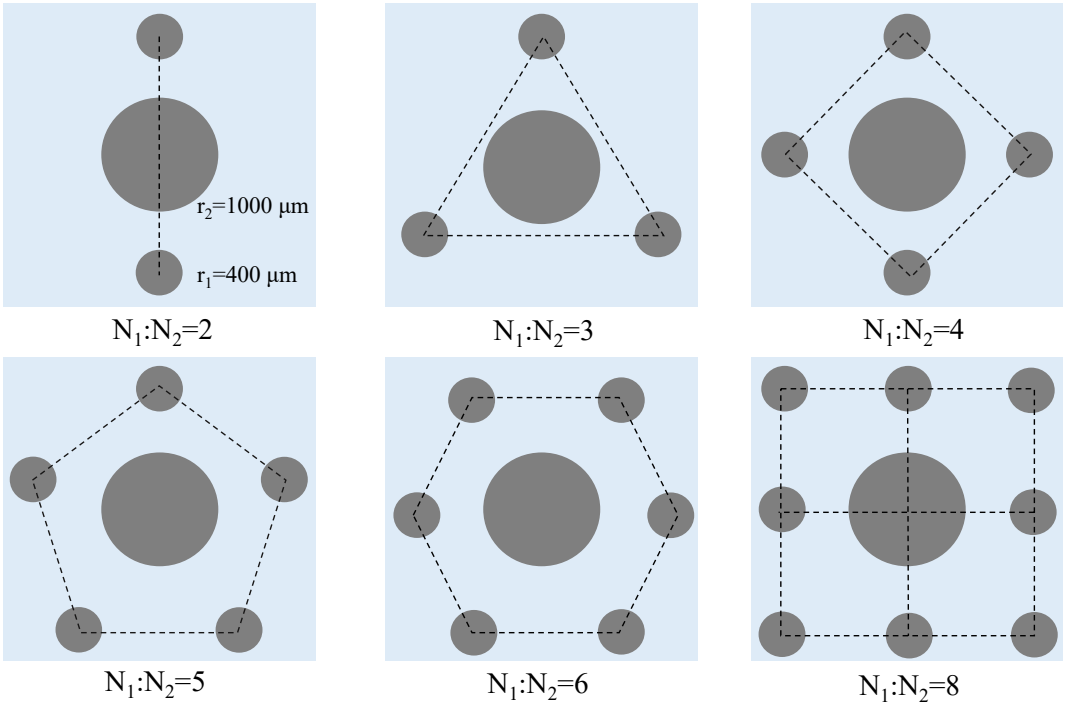

Fig. S10 Different assignments of microchannels and macrochannels.

Section S11. Stability of our evaporator under saturated saline water

As shown in Fig. S11, we have measured the evaporation rate every hour during the 8 hours' test. The evaporation rate can maintain at a stable evaporation rate and it could hardly found any salt crystallization on the evaporation surface, demonstrating the stability of our evaporator to achieve an 8-hour tolerance to saturated saline water.

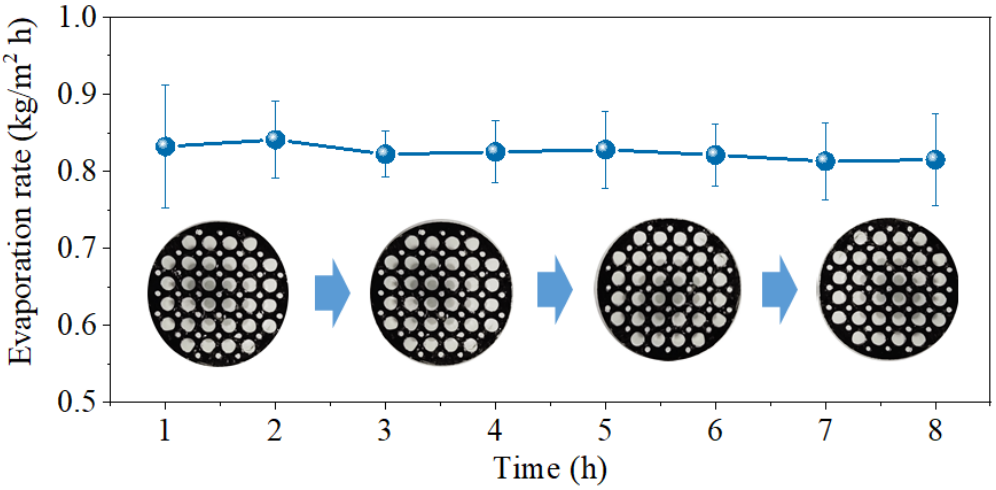

Fig. S11 Stability of our evaporator under saturated saline water.

Section S12. Salt rejecting performance of supersaturated salty water

As presented in Fig. S12, some salt granules are placed on the surface of a bionic absorbers first. During the solar evaporation process, the temperature of surface will be increased, leading to a higher solubility of salt solution. Therefore, the salt granules will be brought back to bulk water, demonstrating an excellent salt rejecting capability.

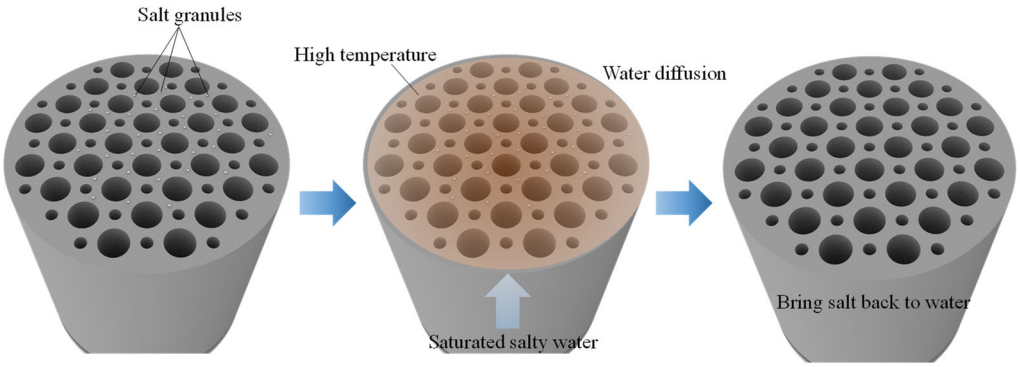

Fig. S12 Salt rejecting performance of our bionic solar evaporators for supersaturated salty water.

Section S13. Parameters for the 3D printing process

Table S1 Parameters of printed resin

Parameters of resin	Value
Hardness (D)	82
Tensile strength (MPa)	38
Elongation (%)	8
Modulus of elasticity (MPa)	1149
Bending strength (MPa)	49
Modulus of bending (MPa)	1476